Received: 16 September 2022 | Revised: 9 November 2022 | Accepted: 5 December 2022

DOI: 10.1111/andr.13361

ANDROLOGY WILEY

ORIGINAL ARTICLE

Intermitochondrial cement (IMC) harbors piRNA biogenesis machinery and exonuclease domain-containing proteins EXD1 and EXD2 in mouse spermatocytes

Opeyemi Olotu[1] | Mark Dowling[2] | David Homolka[2] | Magdalena N. Wojtas[2,3] | Panyi Tran[1] | Tiina Lehtiniemi[1] | Matteo Da Ros[1] | Ramesh S. Pillai[2] | Noora Kotaja[1]

[1]Institute of Biomedicine, Integrative Physiology and Pharmacology Unit, University of Turku, Turku, Finland

[2]Department of Molecular Biology, Science III, University of Geneva, Geneva, Switzerland

[3]Instituto Biofisika (UPV/EHU, CSIC), University of the Basque Country, Leioa, Spain

Correspondence
Noora Kotaja, Institute of Biomedicine, Integrative Physiology and Pharmacology Unit, University of Turku, Kiinamyllynkatu 10, 20520 Turku, Finland.
Email: noora.kotaja@utu.fi

Present address
Magdalena N. Wojtas, Instituto Biofisika (UPV/EHU, CSIC), University of the Basque Country, Leioa, Spain

Abstract

Background: Germ granules are large cytoplasmic ribonucleoprotein complexes that emerge in the germline to participate in RNA regulation. The two most prominent germ granules are the intermitochondrial cement (IMC) in meiotic spermatocytes and the chromatoid body (CB) in haploid round spermatids, both functionally linked to the PIWI-interacting RNA (piRNA) pathway.

Aims: In this study, we clarified the IMC function by identifying proteins that form complexes with a well-known IMC protein PIWIL2/MILI in the mouse testis.

Results: The PIWIL2 interactome included several proteins with known functions in piRNA biogenesis. We further characterized the expression and localization of two of the identified proteins, Exonuclease 3′–5′ domain-containing proteins EXD1 and EXD2, and confirmed their localization to the IMC. We showed that EXD2 interacts with PIWIL2, and that the mutation of Exd2 exonuclease domain in mice induces mis-regulation of piRNA levels originating from specific pachytene piRNA clusters, but does not disrupt male fertility.

Conclusion: Altogether, this study highlights the central role of the IMC as a platform for piRNA biogenesis, and suggests that EXD1 and EXD2 function in the IMC-mediated RNA regulation in postnatal male germ cells.

KEYWORDS
chromatoid body, EXD1, EXD2, intermitochondrial cement, piRNA, spermatogenesis

1 | INTRODUCTION

Spatially and temporally controlled gene expression is a prerequisite for the successful male germ cell differentiation (spermatogenesis) and production of good-quality spermatozoa. Male germ cells are transcriptionally active, and they express their genome broadly; particularly, meiotic spermatocytes and haploid round spermatids have exceptionally diverse transcriptomes, including a wide range of transcripts from intergenic non-annotated regions,[1] as well as enormous amounts of ~30 nucleotides-long germline-specific small non-coding

RNAs, PIWI-interacting RNAs (piRNA).[2–6] These so-called pachytene piRNAs, whose expression is induced at the pachytene stage of meiotic prophase I, are produced from genomic clusters as long precursors that are further processed to small RNAs by the piRNA biogenesis machinery.[7,8] Pachytene piRNAs contribute to about 95% piRNAs in adult mouse testes, and they are found in complexes with the PIWI proteins PIWIL1/MIWI and PIWIL2/MILI. The expressions PIWIL1 and PIWIL2 temporally coincide with pachytene piRNA production, with PIWIL2 being expressed in spermatogenic cells up to early round spermatid phase, and PIWIL1 a bit later in late pachytene spermatocytes and round spermatids.[6,9–11] Unlike piRNAs in embryonic germ cells that have a well-characterized function in silencing transposable elements,[6,12] pachytene piRNAs appear to have more diverse functions, including also regulation of meiotic and post-meiotic non-coding and protein-coding RNAs, as well as in the translational control of mRNAs.[13–15]

The biogenesis and function of piRNAs have been linked to germ cell-specific cytoplasmic ribonucleoprotein granules.[11,16] The two best-characterized and histologically the most prominent germ granules in differentiating male germ cells in mice are the intermitochondrial cement (IMC) and the chromatoid body (CB). IMC appears as a dense material between the clusters of mitochondria, being particularly conspicuous in pachytene spermatocytes.[17] CB precursor granules emerge in late pachytene spermatocytes, coexisting shortly with the IMC. After meiotic divisions in very early haploid cells, the CB condenses to one single structure that remains as a characteristic feature of round spermatids. In elongating spermatids, the CB is transformed to so-called late-CB, splitting into a satellite body and a ringlike structure that distally travels along the axoneme as the mitochondrial sheath develops in the sperm tail.[18]

We have previously revealed the molecular composition of the CB and shown that it contains a broad range of RNA-binding proteins and different RNA species, including mRNAs, long non-coding RNAs and uncharacterized intergenic transcripts.[19–21] piRNAs accumulate in the CB together with PIWI proteins PIWIL1 and PIWIL2 and other proteins implicated in the piRNA pathway, such as a DEAD-box RNA helicase DDX4 and Tudor domain-containing scaffolding proteins TDRD1, TDRD6, and TDRD7.[19–21] The IMC appears earlier than the CB in pachytene spermatocytes during the time of a massive production of pachytene piRNAs.[11] Many proteins involved in the piRNA biogenesis are known to be associated with mitochondria (e.g., mitochondrial membrane proteins PLD6 and GASZ/ASZ1), and they are absent from the CB.[22–24] The current view is that the pachytene piRNA production takes place in the IMC, and the CB serves as a platform for transcriptome regulation, including the piRNA-targeted RNA regulation.[11] However, the full molecular composition of the IMC has not been identified because of challenges in an isolation of these structures, which has hindered the understanding of its role in germline RNA-based mechanisms, and the functional differences between the IMC and the CB.

In this study, we identified proteins that form complexes with the IMC component PIWIL2 in pachytene spermatocytes. We identified several piRNA biogenesis factors in PIWIL2 complexes, highlighting the central role of the IMC in piRNA production. From the PIWIL2-interacting proteins, we selected EXD1 and EXD2 because of their putative catalytic role in IMC-mediated RNA processing for further analysis and characterized their expression and localization during post-natal spermatogenesis. We showed that they both interact with PIWIL2 and localize to the IMC with piRNA biogenesis factors. In contrast, only EXD1 was found in the CB. We also showed that the mutation of the exonuclease domain of *Exd2* in mice induces misregulation of piRNAs from specific clusters without affecting the overall piRNA biogenesis. Altogether, these results substantiate the function of the IMC as a platform for piRNA biogenesis and suggest that EXD proteins operate in the IMC with piRNA biogenesis factors.

2 | MATERIALS AND METHODS

2.1 | Ethical statement

Wild-type C57BL/6NHsd and FVB mice were used to collect tissues for experiments. Mice were grown under pathogen-free conditions and euthanized by carbon dioxide followed by cervical dislocation. Animal experiments were carried out according to Finnish laws and protocols approved by the ethical committee of animal experimentation, University of Turku animal care center, in agreement with good laboratory practice. License number: 2009-1206-Kotaja. *Exd2* mutant mice were generated at the mouse transgenic facility of the EMBL Monterotondo, Rome, Italy. Experiments in Grenoble, France, were covered by an authorization (no. 381007) from the Direction Departementale de la Protection des Populations, Prefecture de l'Isere.

2.2 | Cell Culture and transfection

HeLa cells (CCL-2, American Type Culture Collection) were maintained in Dulbecco's Modified Eagle Medium/Nutrient Mixture F-12 (DMEM/F12) (D-18900, Sigma) supplemented with 10% fetal bovine serum (S1810, Biowest), 1% penicillin/streptomycin (15140-122, Gibco Life Technology) at 37°C in a humidified 5% CO_2 incubator. For transfection, HeLa cells were plated on 6-well culture plate (657160, Greiner Bio-One). On the following day, cells were transfected with 2 μg EXD2 (Myc-DDK-tagged; MR207967, OriGene), 2 μg EXD1 (Myc-DDK-tagged; MR219928, OriGene), and 2 μg MILI-FLAG overexpressing plasmids diluted in OPTI-MEM 1 (1X) (31985-062, Gibco Life Technology). FuGENE HD (E2311/2, Promega) was used as a transfection reagent (ratio 2:1).

2.3 | Immunofluorescence analysis

Mouse testes were collected and fixed in 4% paraformaldehyde in phosphate-buffered saline (PBS) overnight in rotation at room temperature (RT). The fixed samples were dehydrated in 70% ethanol and embedded into paraffin. Testis sections (4 μm) were cut and mounted onto polylysine-coated slides. Sections were deparaffinized as follows:

3 × 5 min xylene, 2 × 10 min 100% ethanol, 2 × 10 min 96% ethanol, 2 × 10 min 70% ethanol, and 2 × 2 min milliQ water. Antigens were retrieved in citrate solution (10 mM sodium citrate, 0.05% Tween 20, pH 6.0) under 1 atm at 120°C for 20 min. For samples stained with anti-EXD1 antibody, antigen heat retrieval was carried out using 10 mM Tris-EDTA 0.05% Tween 20 buffer, pH 9.0. Samples were allowed to cool down at RT washed 4 × 3 min with milliQ water and once with PBS before incubating in blocking solution containing 10% bovine serum albumin in PBS with 0.1% Triton X-100 (PBST) at RT in moist incubation chamber for 1 h. Samples were incubated with primary antibodies diluted in blocking solution at +4°C overnight then washed 3 × 5 min with PBST. Samples were incubated with Alexa Fluor 488/594/647-conjugated secondary antibodies (Life Technologies) (1:1000) in blocking solution at RT for 1 h and washed 3 × 5 min with PBST. Finally, sections were stained with DAPI (1:20000 in PBS, D9542 Sigma-Aldrich, 5 mg/ml stock) and mounted with ProLong Diamond Antifade Mountant (P36970, Life Technologies). Z-stacks immunofluorescence images were acquired with the 3i spinning disk confocal microscope (objective 100 × 1.4 oil, Intelligent Imaging Innovations). Acquired images were processed with 3i SlideBook version 6 (Intelligent Imaging Innovations, USA) and ImageJ 1.48 software version (National Institute of Health, USA). Maximal intensity projections were generated from Z-stacks, and noise removed by background subtraction using ImageJ. Representative images (in Z-stacks) for 3D reconstruction were processed with Imaris software 8.1.2 and were converted to QuickTime videos.

2.4 | Cross-linking and immunoprecipitation

For cross-linking, we used the same conditions as described for the CB isolation in Ref. [21]. Six 15-day-old male mouse testes were collected in PBS, and seminiferous tubules were digested in 0.5 mg/ml collagenase type 1 (LS004196, Worthington Biochemical) in PBS containing 0.1% glucose and 1 µg/ml DNase I (LS006353, Lakewood New Jersey) in rotation at RT for 60 min. Digested tubules were filtered through 100 µm filter (352360; BD biosciences), washed with 0.1% glucose in PBS, and cross-linked with 0.1% (v/v) paraformaldehyde (50-980-487, Thermo Fisher Scientific) at RT for 20 min. Cross-linked cells were centrifuged at 300 × *g* at 4°C for 5 min, supernatant discarded, and cells were lysed by sonication (UCD-200, Diagenode) in 1.5 ml of RIPA buffer (50 mM Tris-HCl at pH 7.5, 1% NP-40, 0.5% w/v sodium deoxycholate, 0.05% w/v sodium dodecyl sulfate, 1 mM EDTA, 150 mM NaCl, 1× complete Mini Protease Inhibitor Cocktail [11836153001; Roche], 0.2 mM PMSFI, and 1 mM DTT) using medium settings for 6 × 30 s intervals. Lysed cells were centrifuged at 300 × *g*, +4°C for 10 min. Supernatant fraction was first pre-cleared with 10 µl of washed Dynabeads Protein G (10446293, Invitrogen), and the pre-cleared lysate was then subjected to immunoprecipitation using beads coupled with 2 µg of antibody or negative control IgG on a vertical rotator at +4°C overnight. The beads–antibody–antigen complexes were washed three times in 1 ml lysis buffer. These complexes were used for mass spectrometry and Western blotting.

2.5 | Co-immunoprecipitation without cross-linking

To study protein–protein interaction in vivo, three 8-week-old male mouse testes were homogenized with TissueLyser LT (69980, QIAGEN) homogenizer in isotonic non-denaturing lysis buffer (50 mM Tris-HCl, pH 8.0, 150 mM NaCl, 5 mM EDTA, 1% Triton X-100, 1X complete Mini Protease Inhibitor Cocktail, 0.2 mM PMSF, and 1 mM DTT). To study the interactions of ectopically expressed proteins, transfected HeLa cells were washed in ice-cold PBS after 24 h and then lysed with the isotonic lysis buffer for 30 min on ice. Both tissue and cell lysates were centrifuged at 17 000 × *g* for 10 min. Cleared supernatant fractions were used for immunoprecipitation as described above.

2.6 | Mass spectrometry

To prepare samples for mass spectrometry, antibody–antigen–bead complexes were washed 3 × 1 ml of 50 mM Tris pH 8, digested, and analyzed at the Turku Proteomics Facility of the Turku Bioscience center using LC–ESI–MS/MS (2X Q Exactive HF mass spectrometer).

2.7 | Western blotting

For expression analysis in tissues and juvenile testes, protein concentrations were measured with Pierce BCA protein assay kit (23227, Life Technologies) and absorbance with Victor X4 plate reader (2030-0050, PerkinElmer). Equal amount of protein lysates were diluted with Laemmli buffer and heated at 95°C for 5 min. Immunoprecipitated protein complexes were eluted in Laemmli buffer by heating at 95°C for 5 min. Proteins were separated by 4%–20%-PAGE (456-1094, Mini-PROTEAN) at 100 V and transferred unto PVDF membrane (10600023, RPN303F, Amersham Hybond), with settings 90 V, 400 mA for 1 h at +4°C. After treating with 100% methanol, membrane was air-dried at RT overnight then incubated with primary antibodies (Table 1) diluted in 5% skimmed milk in PBS containing 0.1% Triton X-100 at RT for 1 h or at +4°C overnight. Membranes were washed 3 × 10 min in PBS containing 0.1% Tween-20 then incubated for 1 h at RT in horseradish peroxide-conjugated anti-rabbit or anti-mouse IgG secondary antibody. Membranes were washed 3 × 10 min in PBS containing 0.1% Tween-20. Proteins were detected by incubating the membrane in western lightening ECL pro (Ne11200IEA, Perkin Elmer) for 1 min. Signals were obtained with LAS 4000 (Fujifilm) or Azure Sapphire Biomolecular Imager (Azure Biosystems) and images saved as 16 bit TIFF files. Images were processed with Adobe Photoshop Creative Suite 5.

2.8 | *Exd2* mutant mice

Genomes of single mouse embryos of the C57BL6 background were edited using guide RNA/Cas9 endonuclease complex (gRNA forward: CACCACTTGGAATTGACTGTGAAT and gRNA reverse: AAACATTCACAGTCAATTCCAAGT) to remove the 3′ end of exon 2 of

TABLE 1 Primary antibodies used in the study

Antibody	Host	Dilution	Cat. no	Manufacturer
EXD2	Rabbit polyclonal	1/200	20138-1-AP	ProteinTech
EXD1	Rabbit polyclonal	1/100	17313-1-AP	ProteinTech
ASZ1	Rabbit polyclonal	1/200	21550-1-AP	ProteinTech
PIWIL2	Mouse monoclonal	1/1000	MABE363	Millipore
Cytochrome C	Mouse monoclonal	1/500	556433	BD Pharmingen
DDX4	Rabbit polyclonal	1/1000	ab13840	Abcam
DDX25	Goat polyclonal	1/200	SC-51271	Santa Cruz
TDRD1	Rat IgG_{2A}	1/50	MAB6296	R&D systems
β-Actin	Mouse monoclonal	1/5000	A1978	Sigma
GAPDH	Mouse monoclonal	1/5000	5G4	HyTest
H2A.X	Mouse monoclonal	1/500	05-636	Millipore
Human VASA (DDX4)	Goat polyclonal	1/1000	AF2030-SP	R&D systems

the mouse *Exd2* gene locus and part of the downstream intron. Mice were genotyped by Sanger sequencing of small testicular biopsies. Small pieces of testes were cut and lysed in 100 µl of lysis buffer (10 mM NaOH, 0.1 mM EDTA pH 8.0) at 95°C for 90 min. After the lysis, the lysates were centrifuged at 3000 rpm for 10 min at RT. The supernatant of 50 µl was transferred to a new tube, and 50 µl of neutralizing solution (20 mM Tris-HCl pH 8.0 and 1 mM EDTA pH 8.0) was added to the supernatant. The mutated region of *Exd2* gene was amplified by PCR in a reaction containing 10 µl Phire Green Hot Start II PCR Master Mix (Thermo Fisher Scientific); 1.0 µl of a primer mix (forward: GATGACCAGCTACCCTTTGGTGCCC, reverse: GAGCTCAGTCTATTCTTGGCCACCC, 10 µM each); 7.0 µl water; 2.0 µl DNA. PCR program: (1) 98°C for 30 s, (2) 98°C for 5 s, (3) 63°C for 5 s, (4) 72°C for 10 s, (5) repeat steps 2–4 35 times, (6) 72°C for 60 s. PCR products were purified with QIAquick PCR Purification Kit (250) (QIAGEN). PCR products were Sanger sequenced by Microsynth. The forward primer was used for Sanger sequencing.

2.9 | RNA extraction and RNA sequencing

RNA was extracted from testes with TRIzol Reagent (Invitrogen). RNA pellets were resuspended in 100 µl RNase free water. RNA concentration was quantified with NanoDrop (Thermo Fisher Scientific). For isolation of small RNAs, 10 µg of total RNA was run into a 15% denaturing urea-PAGE gel, the region of gel-containing small RNAs was cut out, and small RNAs were extracted from the gel by shaking for 4 h at 25°C in 400 µl of 0.4 M NaCl. After incubation, the solution was filtered by spinning full speed for 2 min, and RNA was precipitated by adding 40 µl of 7.5 M ammonium acetate, pH 5.5, 1 µl of Glycogen RNA grade (20 ng/ml) and 1 ml of 100% EtOH, incubating 5 h at −20°C. After centrifugation, RNA pellets were washed with 80% EtOH and suspended in RNase free H_2O for Illumina library preparation. Small RNA-seq libraries were prepared using NEBNext Multiplex Small RNA Library Prep Set for Illumina, and the quality of the libraries were validated in 2% agarose gel. For size selection, libraries were run into a 3.6% agarose (MetaPhor) gel, region of desired size was cut out, and DNA was extracted from gel slices with QIAGEN MinElute Gel extraction Kit. For the preparation of RNA-seq libraries, ribosomal RNA was depleted from 1 µg of total RNA using NEBNext rRNA Depletion Kit v2, and libraries were prepared using NEBNext Ultra II Directional RNA Library Prep Kit for Illumina. Both small RNA-seq and RNA-seq libraries were sequenced at the GENOMICS Platform of the University of Geneva using Illumina HiSeq 4000 platform with single-end run with a read length of 50 nt.

2.10 | RNA-seq data analysis

2.10.1 | Analysis of small RNA-seq libraries

Reads were sorted into individual libraries based on the barcodes, and the 3′ adapter sequences were clipped from the reads using cutadapt (DOI: https://doi.org/10.14806/ej.17.1.200) with only sequences of at least 15 nucleotides left for further analysis (cutadapt parameters: -a AGATCGGAAGAGCACACGTCT -m 15 -e 0.2 -O 4 -q 10–match-read-wildcards). The reads were mapped to the mouse genome (GRCm38: Ensembl release 95) using STAR (parameters: –runThreadN 10–outFilterType BySJout–limitOutSJcollapsed 50000000–limitIObufferSize 1500000000). The reads of 25—32 nt were considered to represent piRNAs and selected for further analysis. To compare the origin of piRNAs, the piRNAs were annotated based on ENSEMBL gene biotypes, position of tRNAs (tRNAs table from UCSC), repeats (rmsk table from UCSC), and pachytene piRNA clusters.[8] Repeat associated piRNAs were further annotated to individual repeat classes. Mapping to consensus sequences of L1_MM and IAPLTR1a_I_MM (RepBase26.08) using bowtie allowing 1 mismatch (parameters: -v 1 -a–best–strata) was used to plot the piRNA distribution along these repeats. To see whether there is the 10 nt overlap between targeting and produced piRNA 5′ ends (ping-pong signature),

we plotted the score for piRNA pairs having specific 5′–5′ end distance Δ. The score refers to the product of the counts of piRNAs with 5′ end distance Δ: score (Δ) = $\sum M(i) \times N(i+\Delta)$ where $M(i)$ is the count of produced piRNAs (in rpm) with 5′ end on the plus strand at a particular position i and $N(i+\Delta)$ is the count of piRNAs which have their 5′ end position at minus strand at $i+\Delta$. The distance equal to 0 refers to a situation where piRNAs share the 5′ end nucleotide and the distance 9 corresponds to 10 nt overlap of piRNA 5′ ends which is characteristic of piRNA ping-pong amplification. To compare the piRNA production from individual pachytene piRNA clusters, the piRNA counts for each cluster were compared between *Exd2*$^{\Delta}$ and *Exd2*$^{+/+}$ using edgeR. In the case of overlapping clusters, only the longest ones were retained. Obtained log2 fold changes with the statistical significance were used to construct the volcano plot.

2.10.2 | Analysis of RNA-seq libraries

Reads were sorted into individual libraries based on the barcodes and mapped to the mouse genome (GRCm38: Ensembl release 95) using STAR (parameters: –runThreadN 10 -outFilterType BySJout–limitOutSJcollapsed 50000000 –limitIObufferSize 1500000000). The read counts for each pachytene piRNA cluster were compared between *Exd2*$^{\Delta}$ and *Exd2*$^{+/+}$ using edgeR. In the case of overlapping clusters, only the longest ones were retained. Obtained log2 fold changes with the statistical significance were used to construct the volcano plot. To verify the deletion in *Exd2*$^{\Delta}$ mice, we checked the presence of TTGGAATTGACTGTGAATGG sequence, which refers to 3′ end of exon 2, in individual libraries. The normalized mean read coverage (rpm) was plotted along the *Exd2* locus to show expression in *Exd2*$^{\Delta}$ and *Exd2*$^{+/+}$ mice. To see how the deletion in *Exd2*$^{\Delta}$ mice affects the final transcript, we plotted the position of the exon 2–3 splice-junctions obtained from STAR SJ.out.tab files. Only uniquely mapped reads were considered with at least five reads abundance across all samples. Although in *Exd2*$^{+/+}$ mice only canonically spliced reads were detected, the deletion in *Exd2*$^{\Delta}$ mice results in aberrant splicing of exon 2 resulting in absence of 3′ end of exon 2 or whole exon 2 skipping (Figure S3F). The most common splicing pattern in *Exd2*$^{\Delta}$ produces intron at chr12:80476090-80480454 resulting in in-frame 33 amino acids deletion, including the DCE motif (Figure S3G).

3 | RESULTS

3.1 | piRNA biogenesis factors gather to the IMC in pachytene spermatocytes

To clarify the composition of the IMC, we identified proteins that form complexes with the known IMC component PIWIL2. As PIWIL2 is known to localize to the CB in addition to the IMC, we avoided CB contamination by using testes collected from 15-day-old mice. At this time point, the first wave of spermatogenesis has progressed until pachytene spermatocyte phase, and CBs have not yet formed. To preserve the IMC structure, testicular cells were mildly cross-linked with 0.1% paraformaldehyde using the conditions optimized for the CB isolation from mouse testes.[20,21] The presence of IMC in the cytoplasm of pachytene spermatocytes at P15 was validated by immunostaining using PIWIL2 antibody (Figure 1A). The lack of CB-containing cells at P15 was validated using an antibody against DDX25, a known CB precursor and CB component[11] (Figure 1A,B).

The mass spectrometric analysis of the mildly cross-linked PIWIL2-complexes identified 64 proteins that were present in both replicate samples but absent in the IgG control and were therefore potential IMC components (Supplementary Table S1). A total of 25 of them have previously been identified as the CB components (Table S1; Figure 1C).[20] GO term analysis revealed that GO terms connected to RNA metabolism and regulation were enriched among the 64 PIWIL2-interacting proteins (Figure 1D; Table S2). A total of 37 proteins were listed under the GO term "RNA metabolic process" (Table S2). Importantly, the GO term "piRNA metabolic process" was enriched (14 proteins), suggesting a central role for the IMC in the piRNA pathway.

Although many CB components (PIWIL2, PIWIL1, DDX4, MAEL, and Tudor domain-containing proteins) have been functionally associated with the piRNA pathway, the core components of the piRNA biogenesis machinery are not found in the CB.[20] Instead, the piRNA biogenesis machinery is found in complexes with PIWIL2 in P15 testes suggesting their presence in the IMC. These proteins include ASZ1, PLD6, MOV10L1, GPAT2, TDRKH, and FKBP6.[6] This finding supports the role of mitochondria-associated IMC as a site for piRNA biogenesis. One of the proteins identified in this study, EXD1, was recently shown to function in complex with TDRD12, promoting piRNA production in embryonic testis.[25,26] Interestingly, another 3′–5′ exonuclease domain-containing protein, EXD2, was also a strong hit in the mass spectrometric analysis. EXD2 has been shown to localize to mitochondrial membranes also in somatic cells.[27,28] Both EXD1 and EXD2 contain a 3′–5′ exonuclease domain (InterPro IPR002562) and they belong to the Ribonuclease H-like superfamily (InterPro IPR012337), but they share very little sequence similarity outside their exonuclease domain (Figure S1A). The function of EXD2 in spermatogenesis and the piRNA pathway has remained unexplored. We validated the interaction of PIWIL2 with EXD2, DDX4, and ASZ1 by immunoprecipitation from P15 testis followed by Western blotting (Figure 1E).

3.2 | EXD2 and EXD1 are prominently expressed in pachytene spermatocytes

To better understand the role of EXD1 and EXD2 in post-natal male germ cells, we characterized their expression and localization during spermatogenesis. We first validated the EXD1 and EXD2 antibodies by Western blotting of cultured HeLa cell extract overexpressing myc-tagged EXD2 and EXD1 (Figure S1B). EXD1 antibody recognized overexpressed EXD1 but not EXD2, and EXD2 antibody recognized overexpressed EXD2 but not EXD1. In addition, EXD2 antibody gave a bit higher molecular weight signal in non-transfected and EXD1-transfected cells, suggesting that EXD2 is endogenously expressed in

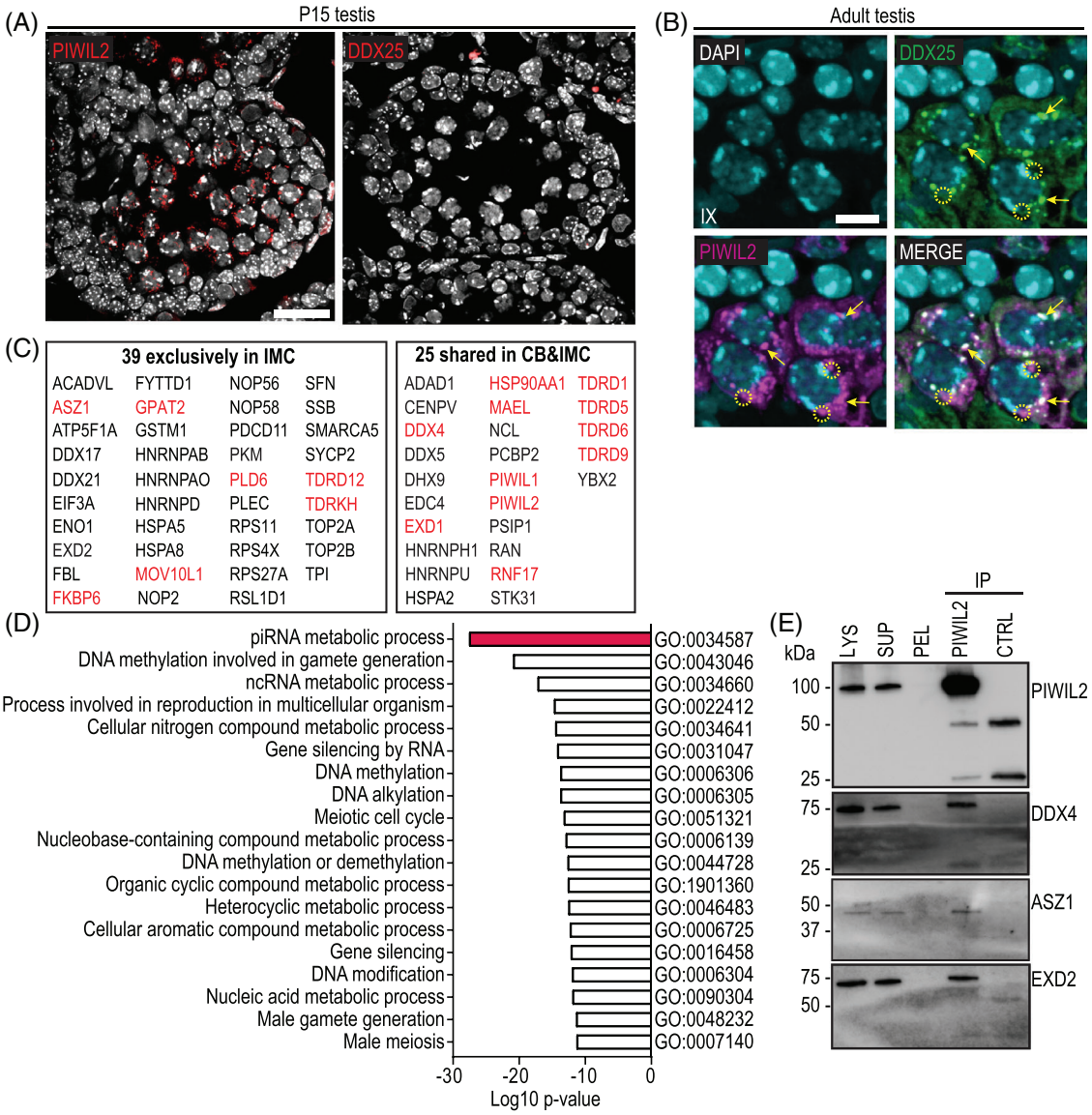

FIGURE 1 Identification of PIWIL2-associated proteins in pachytene spermatocytes. (A) Immunofluorescence with anti-PIWIL2 validated the presence of PIWIL2-positive intermitochondrial cement (IMC) (red) in mid-pachytene spermatocytes in juvenile testes at post-natal day 15 (P15). The absence of DDX25-positive chromatoid body (CB) precursors and CBs was confirmed with anti-DDX25 antibody. DAPI stains nuclei (gray). Scale bar: 25 µm. (B) Immunofluorescence of adult seminiferous tubule cross section at stage IX with anti-DDX25 shows DDX25-positive CB precursors in late pachytene spermatocytes as a positive control for DDX25 staining. PIWIL2 signal (magenta) is found both in DDX25-positive (green) CB precursors (yellow arrows) and IMC (yellow dashed circles). DAPI stains nuclei (cyan). Scale bar: 10 µm. (C) Mass spectrometric analysis of the PIWIL2-complexes immunoprecipitated from cross-linked P15 testes identified 64 proteins as potential IMC components. A total of 25 of them have been earlier identified as CB components. All proteins that have been implicated in the PIWI-interacting RNA (piRNA) pathway[6] are shown in red. (D) Gene ontology (GO) term enrichment analysis. The graph visualized the top 19 enriched biological processes among 64 proteins found in complexes with PIWIL2 in P15 testes. (E) Immunoprecipitation (IP) with anti-PIWIL2 antibody followed by Western blotting validated the interaction of PIWIL2 with DDX4, ASZ1, and EXD2 in P15 testes. Control IP (CTRL) was performed with rabbit IgG. LYS: total cross-linked testicular cell lysate, SUP: the supernatant fraction after low-speed centrifugation that was used as an input for IP, PEL: the pellet fraction after low-speed centrifugation. CBs are so large in size that they are pelleted during low-speed centrifugation. The absence of PIWIL2 and DDX4 in the PEL fraction further validated the absence of CBs in P15 testes

these cells. Western blot analysis of different mouse tissues revealed that the expression of EXD1 and EXD2 is not restricted to the germline (Figure 2A,B). EXD2 is ubiquitously expressed, with strong expression in the testis and heart. The signal in the spleen is very low. EXD1 has high expression in the liver and kidney, and it is also present in other tissues, including the testis. The signal in spleen, brain, and epididymis is very weak.

To characterize the testicular expression of EXD2 and EXD1 in more detail, we collected testes from juvenile mice at different time points during the first wave of spermatogenesis. At birth (P0), testes

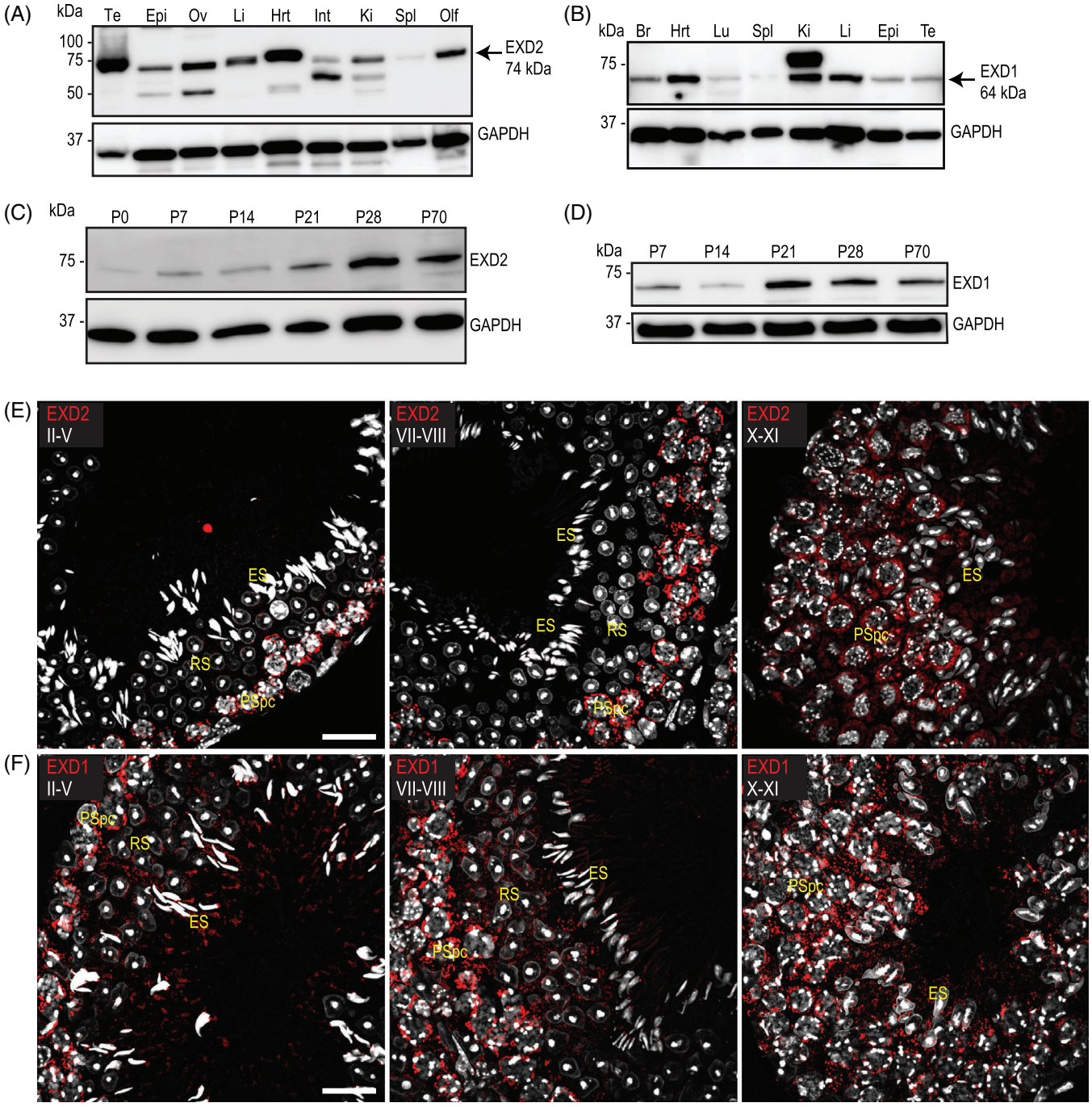

FIGURE 2 Expression of EXD2 and EXD1 in different tissues and during spermatogenesis. Immunoblotting of different tissues with antibodies against (A) EXD2 (74 kDa) and (B) EXD1 (64 kDa). The antibodies detected additional isoforms in some tissues. The isoform of the calculated molecular weight is indicated with an arrow. GAPDH (36 kDa) was used as a loading control. Br, brain; Epi, epididymis; Hrt, heart; Int, intestine; Ki, kidney; Li, liver; Lu, lung; Olf, olfactory epithelium; Ov, ovary; Spl, spleen; Te, testis. (C and D) EXD2 and EXD1 expression during the first wave of spermatogenesis. Testis samples were collected from juvenile mice at different time points (P0, P7, P14, P21, P28, and P70). Anti-GAPDH immunoblotting validated the equal loading of proteins in each lane. (E and F) Adult wild-type C57BL/6 mouse testis sections were immunostained with anti-EXD2 (E) and anti-EXD1 (F) antibodies (red). Nuclei were stained with DAPI (gray). EXD2 signal was mainly detected in the cytoplasm of pachytene spermatocytes (PSpc). The signal was very low in round spermatids (RS) and elongating spermatids (ES). EXD1 localized to the cytoplasm of pachytene spermatocytes and round spermatids. The stage of seminiferous epithelial cycle (II–V, VII–VIII, and X–XI) is indicated for each image. Scale bars: 25 μm. Note that the antigen retrieval in EXD1 staining was carried out in 10 mM Tris-EDTA (pH 9.0), whereas 10 mM citrate buffer (pH 6.0) was used for EXD2 staining

contain only pro-spermatogonia in addition to the somatic cells of the testis. Seven day-old testes (P7) contain proliferating spermatogonia, and in 14-day-old testes (P14), spermatogenesis has progressed until the pachytene phase of the first meiotic prophase. In 21-day-old testes (P21), the first haploid round spermatids have appeared, and in 28-day-old testes (P28), post-meiotic cells have already initiated the nuclear elongation and condensation. Therefore, each time point corresponds to the appearance of a specific spermatogenic cell type. Both EXD1 and EXD2 were expressed at each time point, but the expression increased toward the later time points (Figure 2C,D). Immunofluorescence staining of P0, P7, P14, and P21 testes revealed that the cytoplasmic signals of both proteins are particularly prominent in P14 testes containing pachytene spermatocytes (Figure S1C,D). EXD1 but not EXD2 was also expressed in the cytoplasm of haploid round spermatids at P21 (Figure S1C,D).

Immunofluorescence analysis of adult testes containing full spermatogenesis and all stages of the seminiferous epithelial cycle was performed to obtain cell type-specific information about the expression and localization of EXD2 and EXD1. Both proteins were found in the cytoplasmic compartment, and the signal was not equally distributed but appeared granular (Figure 2E,F). Both proteins were strongly expressed throughout the pachytene phase of meiosis I in early (stages II–V), mid (stages VI–VIII), and late (stages X–XI) pachytene spermatocytes. EXD2 signal disappeared in round spermatids and no signal was detected in elongating spermatids. EXD1 expression pattern appeared very similar to EXD2 in pachytene spermatocytes. However, the EXD1 signal was still found in the cytoplasm of round spermatid, and some signal was also retained in elongating spermatids. To further confirm that the strongest EXD1 and EXD2 expression was specifically in pachytene spermatocytes, testis sections were co-immunostained with anti-γH2AX to visualize the sex body that is a hallmark of this phase of meiotic prophase I (Figure S1E).

3.3 | EXD2 and EXD1 localize to IMC in pachytene spermatocytes

We next performed a detailed co-localization analysis of EXD2 and EXD1 with different germ granule markers. We showed that EXD2, PIWIL2, and another IMC marker TDRD1 co-localize to the cytoplasmic IMC granules in P15 testes that were used as starting material for the identification of PIWIL2-complexes by mass spectrometry (Figure 3A). We also analyzed the co-localizations on adult testes and showed that EXD2 signal almost completely overlap with PIWIL2 signal in the cytoplasmic granules in pachytene spermatocytes (Figure 3B; Movie S1). Furthermore, EXD2 was shown to co-localize with Cytochrome C in pachytene spermatocytes, further validating the localization of EXD2 in the close vicinity of mitochondrial clusters and therefore, to the IMC (Figure 3C). In very late pachytene spermatocytes, another type of germ granule, CB precursor, appears. CB precursors serve as material for the CB that condenses to its final form right after meiosis in early haploid cells.[11] PIWIL2 localizes to both IMC and CB, but some proteins like a DEAD-box helicase DDX25 has CB-restricted localization.[11] We used DDX25 as a CB precursor marker to show that EXD2 did not localize to CB precursors in late spermatocytes (Figure 3D). Furthermore, co-immunofluorescence staining of early round spermatids at stage I–II of the seminiferous epithelial cycle with EXD2 and PIWIL2 revealed that the PIWIL2-positive CBs were lacking the EXD2 signal (Figure 3E). Therefore, the localization of EXD2 is restricted to the mitochondria-associated IMC, consistent with its mitochondrial localization in somatic cells.[27,28]

Like EXD2, EXD1 was also shown to localize to the IMC by co-immunostaining with antibodies against PIWIL2 and TDRD1 (Figure 4A). Interestingly, in contrast to EXD2, EXD1 localization was not restricted to the mitochondria-associated IMC, but co-localization with DDX25 revealed that it is also found in CB precursors in late pachytene spermatocytes (Figure 4B), as well as in the CB in round spermatids (Figure 4C). The localization to both the IMC and CB was also validated with another germ granule marker, DDX4 that is present in both IMC and CB (Figure S2). This is in-line with the earlier identification of EXD1 (but not EXD2) as a CB component by mass spec analysis of isolated CBs[20] (Table S1).

3.4 | Germ granule environment is not required for the interaction of EXD2 with PIWIL2

The original immunoprecipitation for the identification of the proteins forming complexes with PIWIL2 was performed from cross-linked testicular cells to better retain the integrity of the IMC. To study, if EXD proteins are more directly associated with PIWIL2 or other IMC components, we performed immunoprecipitations from adult testes without cross-linking to identify EXD1 and EXD2 interacting proteins by mass spectrometry. PIWIL2 and DDX4 were shown to interact with both EXD1 and EXD2 even without cross-linking (Tables S3 and S4). Furthermore, many additional piRNA pathway proteins, including TDRKH, TDRD1, PIWIL1, TDRD6, ASZ1, and MOV10L1, were found in complex with EXD2 (Table S4). The interaction of EXD2 with PIWIL2, DDX4, and ASZ1 was further validated by co-immunoprecipitation followed by Western blotting (Figure 5A). This indicates that EXD2 forms stable complexes with these proteins in the mouse testis. We also showed that EXD2 and PIWIL2 interact when overexpressed in cultured somatic cells, therefore demonstrating that germ granule environment is not required for their interaction (Figure 5B). The *Exd2* cDNA used in the interaction study encodes a truncated protein lacking the first 150 amino acids, including the motif required for its exonuclease activity.[28,29] Therefore, the interaction of EXD2 with PIWIL2 is not dependent on its catalytic domain.

3.5 | Mutation of *Exd2* affects piRNA levels from specific clusters

To examine the physiological role of EXD2, we engineered a precise deletion to remove the 3′ end of exon 2 of the mouse *Exd2* gene locus and part of the downstream intron (Figure S3A). This deletion removed

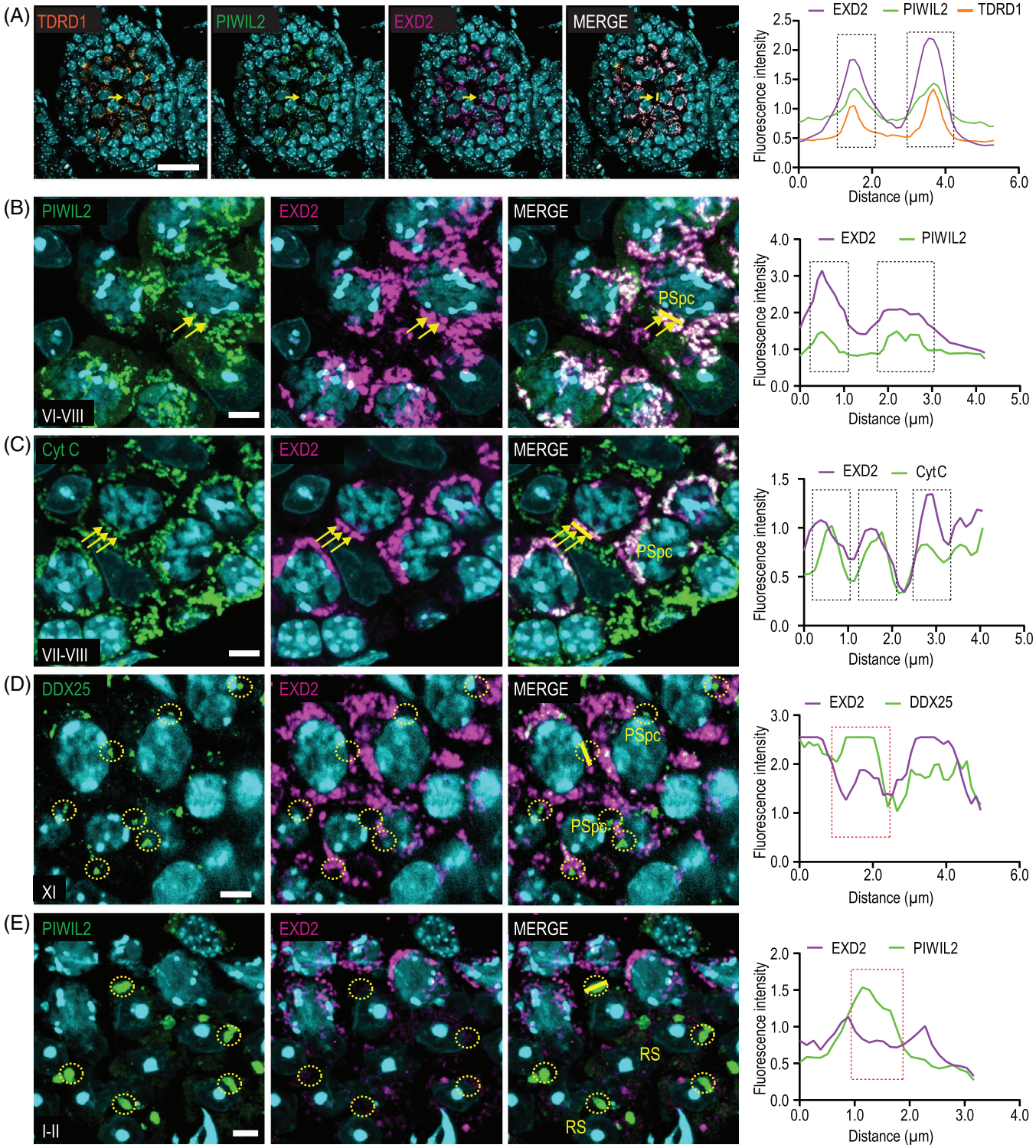

FIGURE 3 EXD2 localizes to the intermitochondrial cement (IMC) but not to the chromatoid body (CB). (A) Co-localization of PIWIL2 (green), TDRD1 (orange), and EXD2 (magenta) to same cytoplasmic granules on PFA-fixed paraffin-embedded P15 testis sections. Nuclei were stained with DAPI (cyan). Scale bar: 25 μm. (B and C) Co-localization of EXD2 (magenta) and (B) PIWIL2 (green) or (C) cytochrome C (Cyt C, green) to the IMC of pachytene spermatocytes (PSpc) on PFA-fixed paraffin-embedded adult testis sections (stage VI–VIII). Yellow arrows point to selected granules with co-localization. Scale bar: 5 μm. (D) EXD2 (magenta) signal does not overlap with DDX25-positive CB precursors (green) in late pachytene spermatocytes at stage XI. Dashed circles indicate a few representative CB precursor granules that are negative for EXD2. Scale bar: 5 μm. (E) EXD2 (magenta) is not found in PIWIL2-positive CBs (green) in round spermatids (RS) at stage I–II. Dashed circles indicate CBs that were negative for EXD2 signal. Scale bar: 5 μm. The line graphs on the right show the fluorescence intensity profiles of different fluorescent colors. Co-localization is shown along the yellow line indicated in the merged images. Shared intensity peaks indicating the co-localization are marked with black dashed boxes (A–C), whereas the absence of co-localization is marked with red dashed boxes (D and E)

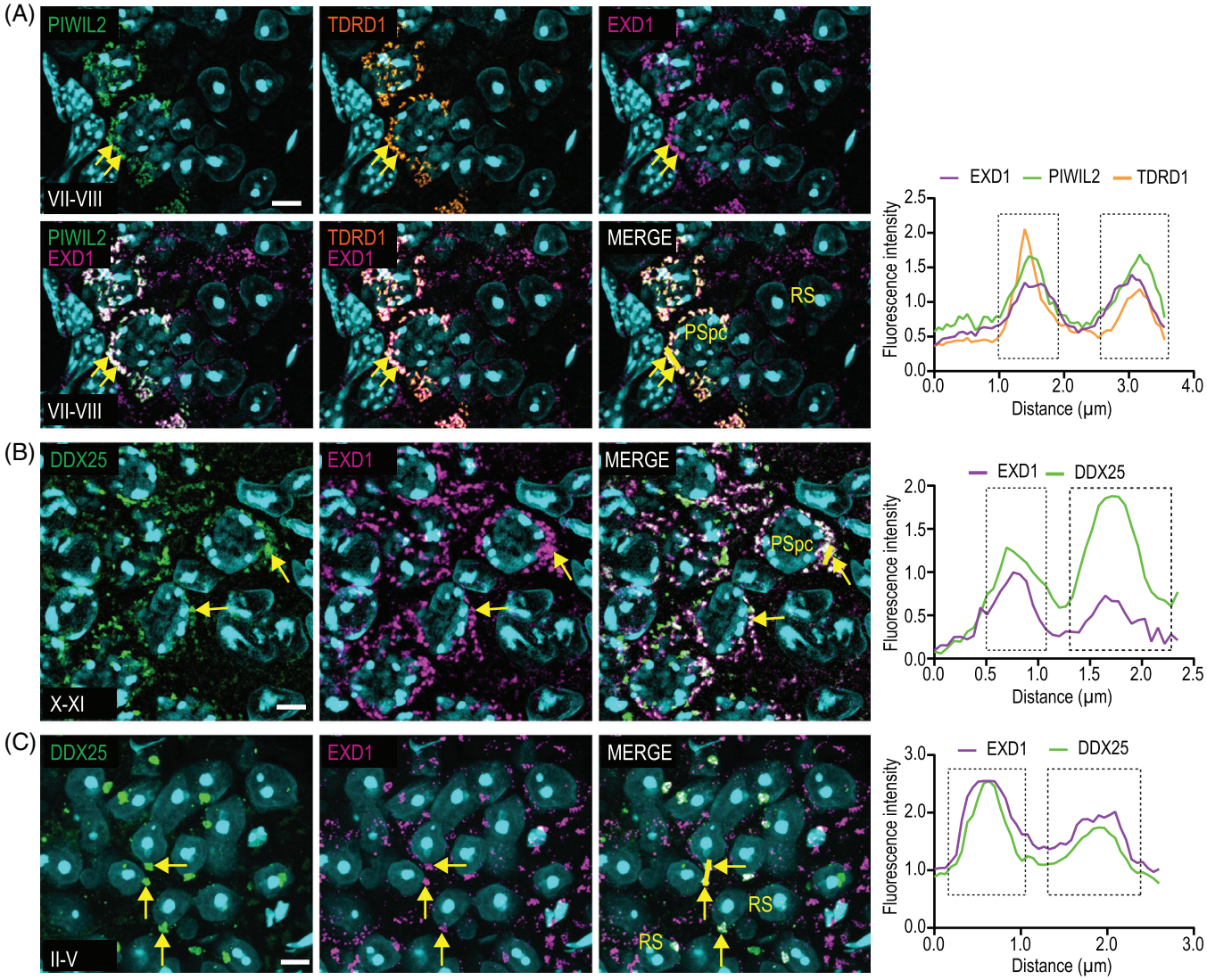

FIGURE 4 EXD1 localizes to the intermitochondrial cement (IMC) and chromatoid body (CB). (A) Co-localization of EXD1 (magenta), PIWIL2 (green), and TDRD1 (orange) in pachytene spermatocytes (PSpc) at stage VII–VIII. RS: round spermatid. Nuclei were stained with DAPI (cyan). Scale bar: 5 μm. Yellow arrows point to selected granules with co-localization. (B and C) Co-localization of EXD1 (magenta) with DDX25 (green) to CB precursors in late pachytene spermatocytes at stage X–X (B), and CBs in round spermatids (RS) at stage II–V (C). Some examples of the EXD1-positive CB precursors (B) and CBs (C) are indicated with yellow arrows. Scale bar: 5 μm. The line graphs on the right show the fluorescence intensity profiles of different fluorescent colors. Co-localization is shown along the yellow line indicated in the merged images. Shared intensity peaks indicating the co-localization are marked with black dashed boxes

the metal-binding sites Asp137 and Glu139 within the DCEW motif has been shown to be required for its 3′ → 5′ exonuclease activity on both DNA and RNA.[28,29] The resulting *Exd2* deletion allele will be hereafter referred to as the *Exd2*$^{\Delta}$ and the WT as *Exd2*$^{+/+}$.

Heterozygous and homozygous *Exd2*$^{\Delta}$ animals were viable, and we did not observe any obvious phenotypes. Visual examination of the testes showed normal size of the *Exd2*$^{\Delta}$ testes (Figure 5C), and the mutant male mice were fertile. To study the effects of *Exd2* mutation on testicular RNA expression, we performed RNA sequencing for adult (>P60) testes from two independent non-littermate males of the homozygous *Exd2*$^{\Delta}$ genotype as well as two age-matched non-littermate wild-type C57BL6 animals as controls. The normal testicular size and fertility allowed us to use adult testes for the analysis because of similar testicular cell composition between the mutant and control animals. We prepared both size-selected (20–40 nt) testicular small RNA libraries and total RNA libraries after ribosomal RNA depletion (Figure S3B,C). The analysis of *Exd2* expression from the RNA-seq data showed similar expression in *Exd2*$^{\Delta}$ and *Exd2*$^{+/+}$ (Figure S3D) but confirmed the lack of reads from the DCE motif in *Exd2*$^{\Delta}$ (Figure S3E), where the splicing of the remaining exon 2–3 produces a mutant RNA having an in-frame deletion of 33 amino acids from the protein (Figure S3F,G).

Next we analyzed small RNAs to investigate the status of the piRNA pathway in the *Exd2*$^{\Delta}$ animals. A length distribution profile revealed a major peak at 30 nt in both control and *Exd2*$^{\Delta}$ libraries (Figure 5D), which likely corresponds to the abundant PIWIL1-bound pachytene

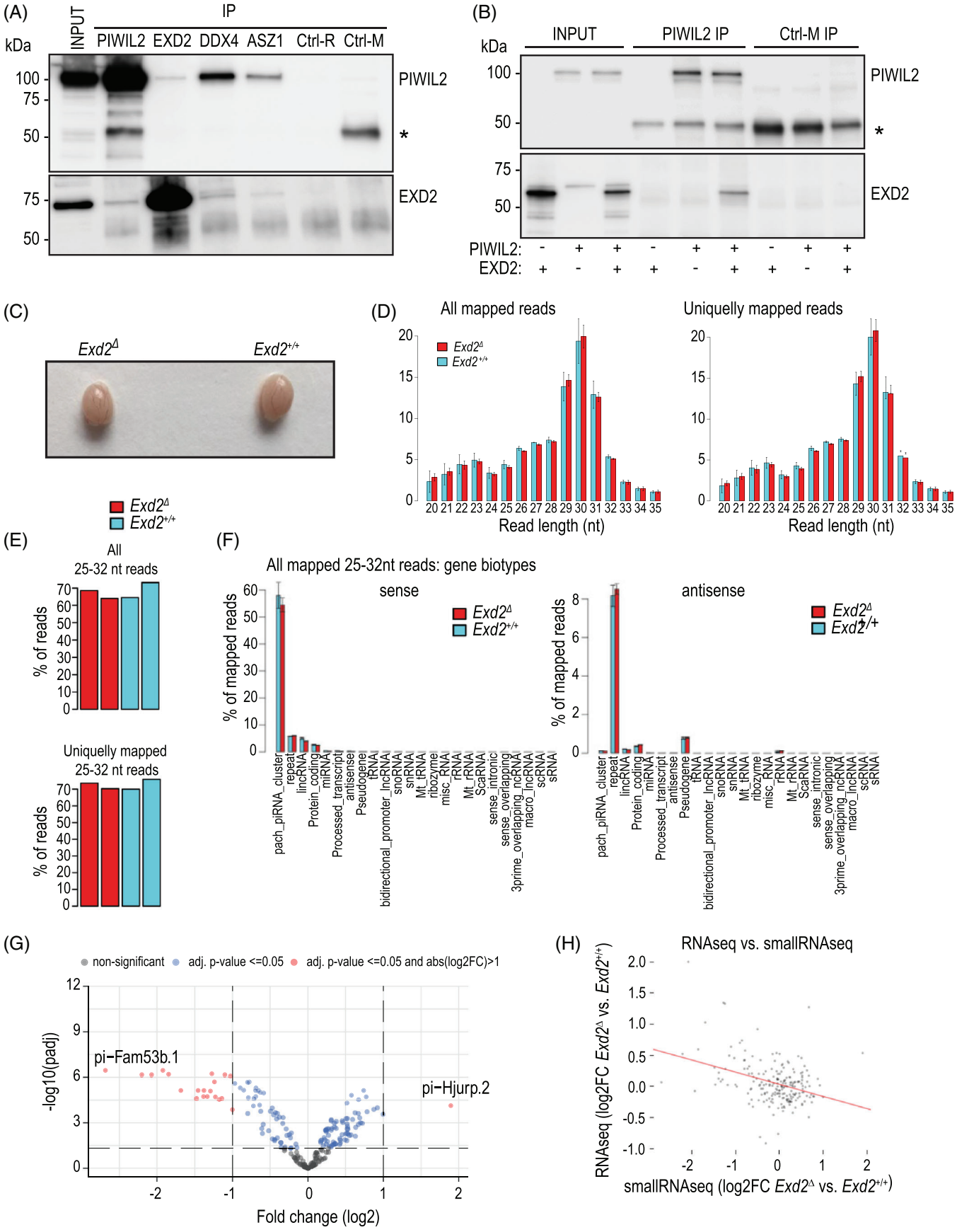

FIGURE 5 EXD2 interacts with PIWIL2 and affects the expression of specific PIWI-interacting RNA (piRNA) clusters. (A) EXD2 interacts with PIWIL2, DDX4, and ASZ1 in adult testis. The immunoprecipitation (IP) was performed from adult mouse testicular cells without cross-linking using

piRNAs. We did not observe any difference in overall levels of piRNAs (Figure 5E). Mapping of the 25–32 nt reads, representing bona fide piRNAs, to the mouse genome showed that most (~60%) reads are sense reads originating from the annotated pachytene piRNA clusters, with the remaining sense reads coming from repeats and protein-coding sequences (Figure 5F). Antisense sequences formed a minority of the mapped reads, with ~8% mapping to the repeat regions (Figure 5F). The proportion of piRNAs mapping to clusters and repeats was similar between the two genotypes. Sorting of the repeat reads into individual transposon classes showed no major difference between the control and *Exd2*$^{\Delta}$ (Figure S4A). Furthermore, we did not observe any differences in the distribution of the repeat reads along the LINE and LTR repeat consensus (Figure S4B), and the 10-nt ping-pong signature between overlapping sense and antisense reads mapping to these consensus sequences was present in both genotypes (Figure S4C).

When the abundance of small RNAs (25–32 nt) mapping to individual pachytene piRNA clusters[8] was examined, we observed several clusters with misregulated levels of primary piRNAs (sense orientation) in the mutant (Figure 5G; Table S5). Twenty clusters were downregulated (log2FC <-1, padj ≤ 0.05), whereas only one cluster was upregulated (log2FC > 1, padj ≤ 0.05) (Figure 5G). The analysis of piRNA precursor transcripts from RNA-seq data revealed that the precursors for the downregulated clusters are not downregulated (Figure S4D; Table S6). This suggests that the production of pachytene piRNA precursors is not affected in *Exd2*$^{\Delta}$, and therefore, the reduced amount of piRNAs from these clusters cannot be explained by the reduced amount of precursors. We also observed a slight negative correlation between the abundance of piRNA levels and that of long precursor reads (Figure 5H). Although this might indicate a role of EXD2 in processing of the piRNA precursors from selected pachytene clusters, the precise molecular mechanism involved is unclear.

4 | DISCUSSION

The presence of germ granules in the cytoplasm of differentiating male germ cells was already discovered at the end of 1800s,[30] but their functions in the germline-specific RNA regulation have only recently started to be uncovered. In this study, we clarified the molecular composition of the mitochondria-associated germ granule, the IMC, by identifying proteins that form complexes with the IMC protein PIWIL2 in P15 testes. Although we cannot exclude the possibility that some of the identified proteins interact with PIWIL2 elsewhere in the cytoplasm, the prominent localization of PIWIL2 to the IMC suggests that the majority of these interactions originate from the IMC. Importantly, our samples were free of CB contamination because we used P15 testes lacking the CB-containing cell types as starting material. We showed that the proteins involved in the biogenesis of piRNAs are enriched in the IMC. Furthermore, detailed characterization of the two identified proteins, EXD1 and EXD2, validated their co-localization with the piRNA pathway proteins to the IMC. EXD2 was shown to interact with PIWIL2, and whereas the mutation of *Exd2* exonuclease domain did not affect overall piRNA biogenesis, it caused misregulation of piRNAs from specific piRNA clusters, suggesting that EXD2 is functionally linked to the piRNA pathway.

The IMC and CB have morphological differences, the most striking being the association with mitochondria, whereas IMC appears as a glue between mitochondrial clusters, and CB is not specifically associated with mitochondria.[11,17] In addition, these granules are temporally separated, and IMC is the most conspicuous in meiotic pachytene spermatocytes, whereas CB condenses to its final form only after meiotic divisions. However, for a short time, these two germ granules coexist in late pachytene/diplotene spermatocytes before the disintegration of mitochondrial clusters and IMC.[11] In this study, we provided novel insight into the functional differences of these granules by comparing their proteomes. We showed that only around 40% of the IMC components are also found in the CB proteome. These shared proteins include many factors implicated in the piRNA pathway (e.g., DDX4, PIWIL2, TDRD1, MAEL, EXD1, and MOV10L1)[20]; however, we showed that the factors specifically involved in piRNA biogenesis (e.g., PLD6, GPAT2, ASZ1, FKBP6, and TDRKH)[6] were found in the IMC only. Many of them have been shown to localize to mitochondrial membranes.[22–24,31–34] Therefore, it appears that the association with mitochondria defines the function of IMC in piRNA production.

Among the PIWIL2-interacting proteins, we identified two 3′–5′ exonuclease domain-containing proteins EXD1 and EXD2. EXD1 has previously been shown to function as piRNA biogenesis factor in embryonic germ cells, where it forms an adaptor complex

antibodies against PIWIL2, EXD2, DDX4, and ASZ1. Rabbit IgG (Ctrl-R) and mouse IgG (Ctrl-M) were used as negative controls. Western blotting detection was performed with anti-PIWIL2 and anti-EXD2 antibodies. (B) Interaction between ectopically overexpressed EXD2 and PIWIL2 in HeLa cells. HeLa cells were transfected with the plasmids encoding PIWIL2 and EXD2 as indicated in the figure. Immunoprecipitation was performed with anti-PIWIL2, and mouse IgG (Ctrl-M) was used as a negative control. The samples were detected with anti-PIWIL2 and anti-EXD2 antibodies. Note that the transfected plasmid encodes an N-terminally truncated EXD2 that migrates at lower molecular weight compared to endogenous EXD2 in the testis (A). An asterisk in (A and B) indicates the signal from the IgG heavy chain. (C) Testicular size of *Exd2* mutant (*Exd2*$^{\Delta}$) and control (*Exd2*$^{+/+}$) mice. (D) Size distribution of all mapped small RNA-seq reads and uniquely mapped reads in *Exd2*$^{\Delta}$ and *Exd2*$^{+/+}$ testes. The error bars refer to range of values from two biological replicates. (E) Amount of all mapped 25–32 nt reads and uniquely mapped 25–32 nt reads in *Exd2*$^{\Delta}$ and *Exd2*$^{+/+}$ testes. (F) Distribution of all mapped 25–32 nt sense and antisense small RNA-seq reads between annotation categories. (G) Volcano plot showing a differential expression of piRNAs originating from distinct pachytene piRNA clusters in *Exd2*$^{\Delta}$ versus *Exd2*$^{+/+}$ testes. Gray dots: nonsignificant, blue dots: padj ≤ 0.05, red dots: padj ≤ 0.05 and log2FC > 1 or <-1. (H) Comparison between the log2FC (*Exd2*$^{\Delta}$ vs. *Exd2*$^{+/+}$) of piRNA precursors from RNA-seq and corresponding log2FC from small RNA-seq data. The dots refer to individual pachytene piRNA clusters. Pearson correlation: −0.36, R^2: 0.13, *p*-value: 8.90e − 08

with PIWIL4/MIWI2 and TDRD12 to enhance the production of piRNAs and suppression of transposons to protect germline genome integrity.[25,26] The deletion of *Exd1* in mice caused a reduction in PIWIL4-associated piRNAs but did not affect spermatogenesis. However, the deletion of *Exd1* in *Tdrd12* heterozygous background greatly inhibited PIWIL4-associated piRNA production, leading to the derepression of retrotransposons and male infertility.[25] Although these studies focused on embryonic germ cells, here we showed that EXD1 is also expressed during post-natal spermatogenesis where it localizes to germ granules. Interestingly, the EXD1 interaction partner TDRD12 was specifically found in IMC, whereas many other TDRD proteins (TDRD1, TDRD5, TDRD6, and TDRD9) were also present in CB, suggesting that EXD1-TDRD12 complex function in piRNA biogenesis pathway in IMC of pachytene spermatocytes. PIWIL4 is only expressed in embryonic germ cells,[35] but two other PIWI proteins PIWIL1 and PIWIL2 localize to both IMC and CB during post-natal spermatogenesis.

EXD2 has previously been reported to localize exclusively to the outer mitochondrial membrane in somatic cultured cells, where it supports mitochondria dynamics.[36] EXD2 has also been reported to be involved in the control of mitochondrial translation, and it is required for normal development and female fertility in *Drosophila melanogaster*.[28] EXD2 appears to have an important role in development and health, as its deficiency has been linked to various defects such as congenital heart problems, brachydactylic, and intellectual disability in humans.[37] According to our results, the mitochondrial localization of EXD2 is conserved in mouse male germ cells, and EXD2 was prominently co-localized to mitochondria-associated IMC. Furthermore, its expression was downregulated in late meiotic cell when IMC disintegrates, and in contrast to EXD1, EXD2 was not found in CB that is not associated with mitochondria.

The available testis samples of the *Exd2* mutant mouse line allowed us to analyze piRNAs in *Exd2*-defective background. It has to be noted that our mouse line is not a full knockout but a mutant EXD2 with internal deletion may be expressed. The deleted region covers the DCE motif shown to be critical for the 3′ → 5′ exonuclease activity on both DNA and RNA,[28,29] but we cannot rule out the possibility that the other remaining regions are sufficient for some functions of EXD2, including the potential cooperation with the piRNA pathway. We showed that EXD2 exonuclease activity is not required for piRNA production as a comparable amount of pachytene piRNAs were produced in control and *Exd2* mutant testes. Although the overall piRNA biogenesis was not affected in the *Exd2* mutant, we did observe imbalance in the piRNA production, and the number of piRNAs produced from 20 piRNA clusters were significantly reduced. The unchanged levels of the precursor transcripts suggest that the reduced number of piRNAs originate from defective piRNA processing from these specific clusters. This intriguing finding together with the accumulation of EXD2 in the IMC with the piRNA biogenesis factors creates interest for further studies to clarify the mechanistic details of the potential involvement of EXD2 in the piRNA biogenesis.

Altogether, our results provide novel evidence about the subcellular compartmentalization of piRNA biogenesis factors in the IMC and the functional differences between the two types of germ granules, the IMC and the CB, in differentiating male germ cells. Furthermore, the presence of the two exonuclease domain-containing proteins EXD1 and EXD2 in the IMC further substantiates the central role of this intriguing mitochondria-associated granule in germline-specific RNA regulation during spermatogenesis.

AUTHOR CONTRIBUTIONS

Conceptualization; investigation; and visualization: Opeyemi Olotu. *Investigation*: Mark Dowling, Magdalena N. Wojtas, Panyi Tran, Tiina Lehtiniemi, Matteo Da Ros. *Data curation; formal analysis; software; and visualization*: David Homolka. *Conceptualization; resources; and supervision*: Ramesh S. Pillai. *Conceptualization; funding acquisition; project administration; resources; supervision; and visualization*: Noora Kotaja. All authors participated in the preparation and editing of the manuscript.

ACKNOWLEDGMENTS

We would like to thank all Kotaja lab members for their support and help. The Turku BioScience Cell Imaging and Proteomics Core Facilities are acknowledged for their services and Turku Center for Disease Modeling (TCDM) and Turku Central Animal Facility for providing expertise on animal experimentation. This study was supported by the Academy of Finland, the Sigrid Jusélius Foundation, the Novo Nordisk Foundation, the Jalmari and Rauha Ahokas Foundation, Turku Doctoral Programme of Molecular Medicine (TuDMM), and the Finnish Cultural Foundation.

CONFLICT OF INTEREST

The authors have nothing to disclose.

DATA AVAILABILITY STATEMENT

All deep sequencing data generated in this study and deposited with the Gene Expression Omnibus (GEO) under the accession number GSE194043.

ORCID

Noora Kotaja https://orcid.org/0000-0003-1503-9170

REFERENCES

1. Soumillon M, Necsulea A, Weier M, et al. Cellular source and mechanisms of high transcriptome complexity in the mammalian testis. *Cell Rep*. 2013;3(6):2179-2190. https://doi.org/10.1016/j.celrep.2013.05.031
2. Girard A, Sachidanandam R, Hannon GJ, Carmell MA. A germline-specific class of small RNAs binds mammalian Piwi proteins. *Nature*. 2006;442(7099):199-202. https://doi.org/10.1038/nature04917
3. Lau NC, Seto AG, Kim J, et al. Characterization of the piRNA complex from rat testes. *Science*. 2006;313(5785):363-367. https://doi.org/10.1126/science.1130164
4. Grivna ST, Pyhtila B, Lin H. MIWI associates with translational machinery and PIWI-interacting RNAs (piRNAs) in regulating spermatogenesis. *Proc Natl Acad Sci USA*. 2006;103(36):13415-13420. https://doi.org/10.1073/pnas.0605506103

5. Aravin A, Gaidatzis D, Pfeffer S, et al. A novel class of small RNAs bind to MILI protein in mouse testes. *Nature*. 2006;442(7099):203-207. https://doi.org/10.1038/nature04916
6. Ozata DM, Gainetdinov I, Zoch A, O'Carroll D, Zamore PD. PIWI-interacting RNAs: small RNAs with big functions. *Nat Rev Genet*. 2019;20(2):89-108. https://doi.org/10.1038/s41576-018-0073-3
7. Ozata DM, Gainetdinov I, Zoch A, O'Carroll D, Zamore PD. PIWI-interacting RNAs: small RNAs with big functions. *Nat Rev Genet*. 2018;20(2):89-108. https://doi.org/10.1038/s41576-018-0073-3
8. Li XZ, Roy CK, Dong X, et al. An ancient transcription factor initiates the burst of piRNA production during early meiosis in mouse testes. *Mol Cell*. 2013;50(1):67-81. https://doi.org/10.1016/j.molcel.2013.02.016
9. Deng W, Lin H. miwi, a murine homolog of piwi, encodes a cytoplasmic protein essential for spermatogenesis. *Dev Cell*. 2002;2(6):819-830.
10. Kuramochi-Miyagawa S, Kimura T, Ijiri TW, et al. Mili, a mammalian member of piwi family gene, is essential for spermatogenesis. *Development*. 2004;131(4):839-849. https://doi.org/10.1242/dev.00973; dev.00973 [pii]
11. Lehtiniemi T, Kotaja N. Germ granule-mediated RNA regulation in male germ cells. *Reproduction*. 2018;155(2):R77-R91. https://doi.org/10.1530/REP-17-0356
12. Castaneda J, Genzor P, Bortvin A. piRNAs, transposon silencing, and germline genome integrity. *Mutat Res*. 2011;14:95-104. May 11 [Ep]. https://doi.org/10.1016/j.mrfmmm.2011.05.002
13. Zhang P, Kang J-Y, Gou L-T, et al. MIWI and piRNA-mediated cleavage of messenger RNAs in mouse testes. *Cell Res*. 2015;25(2):193-207. https://doi.org/10.1038/cr.2015.4
14. Dai P, Wang X, Gou LT, et al. A translation-activating function of MIWI/piRNA during mouse spermiogenesis. *Cell*. 2019;179(7):1566-1581.e16. https://doi.org/10.1016/j.cell.2019.11.022
15. Goh WSS, Falciatori I, Tam OH, et al. piRNA-directed cleavage of meiotic transcripts regulates spermatogenesis. *Genes Dev*. 2015;29(10):1032-1044. https://doi.org/10.1101/GAD.260455.115
16. Eddy EM. Germ plasm and the differentiation of the germ cell line. *Int Rev Cytol*. 1976;43:229-280. https://doi.org/10.1016/S0074-7696(08)60070-4
17. Fawcett DW, Eddy EM, Phillips DM. Observations on the fine structure and relationships of the chromatoid body in mammalian spermatogenesis. *Biol Reprod*. 1970;2(1):129-153.
18. Shang P, Baarends WM, Hoogerbrugge J, et al. Functional transformation of the chromatoid body in mouse spermatids requires testis-specific serine/threonine kinases. *J Cell Sci*. 2010;123(pt 3):331-339. https://doi.org/10.1242/jcs.059949
19. Meikar O, Da Ros M, Liljenbäck H, Toppari J, Kotaja N. Accumulation of piRNAs in the chromatoid bodies purified by a novel isolation protocol. *Exp Cell Res*. 2010;316(9):1567-1575. https://doi.org/10.1016/j.yexcr.2010.02.023
20. Meikar O, Vagin V V, Chalmel F, et al. An atlas of chromatoid body components. *RNA*. 2014;20(4):483-495. https://doi.org/10.1261/rna.043729.113
21. Meikar O, Kotaja N. Isolation of chromatoid bodies from mouse testis as a rich source of short RNAs. *Methods Mol Biol*. 2014;1173:11-25. https://doi.org/10.1007/978-1-4939-0931-5_2
22. Huang H, Gao Q, Peng X, et al. piRNA-associated germline nuage formation and spermatogenesis require MitoPLD profusogenic mitochondrial-surface lipid signaling. *Dev Cell*. 2011;20(3):376-387. https://doi.org/10.1016/j.devcel.2011.01.004
23. Watanabe T, Chuma S, Yamamoto Y, et al. MITOPLD is a mitochondrial protein essential for nuage formation and piRNA biogenesis in the mouse germline. *Dev Cell*. 2011;20(3):364-375. https://doi.org/10.1016/j.devcel.2011.01.005
24. Ma L, Buchold GM, Greenbaum MP, et al. GASZ is essential for male meiosis and suppression of retrotransposon expression in the male germline. *PLoS Genet*. 2009;5(9):e1000635. https://doi.org/10.1371/journal.pgen.1000635
25. Pandey RR, Homolka D, Olotu O, Sachidanandam R, Kotaja N, Pillai RS. Exonuclease domain-containing 1 enhances MIWI2 piRNA biogenesis via its interaction with TDRD12. *Cell Rep*. 2018;24(13):3423-3432.e4. https://doi.org/10.1016/J.CELREP.2018.08.087
26. Yang Z, Chen K-M, Pandey RR, et al. PIWI slicing and EXD1 drive biogenesis of nuclear piRNAs from cytosolic targets of the mouse piRNA pathway. *Mol Cell*. 2016;61:138-152. https://doi.org/10.1016/j.molcel.2015.11.009
27. Park J, Lee SY, Jeong H, et al. The structure of human EXD2 reveals a chimeric 3' to 5' exonuclease domain that discriminates substrates via metal coordination. *Nucleic Acids Res*. 2019;47(13):7078-7093. https://doi.org/10.1093/NAR/GKZ454
28. Silva J, Aivio S, Knobel PA, et al. EXD2 governs germ stem cell homeostasis and lifespan by promoting mitoribosome integrity and translation. *Nat Cell Biol*. 2018;20(2):162-174. https://doi.org/10.1038/s41556-017-0016-9
29. Broderick R, Nieminuszczy J, Baddock HT, et al. EXD2 promotes homologous recombination by facilitating DNA end resection. *Nat Cell Biol*. 2016;18:271.
30. Benda C. Neue mitteilungen über die entwickelung der genitaldrüsen und die metamorphose der samenzellen (histogenese der spermatozoen). Verhandlungen der berliner physiologischen gesellschaft. *Arch Anat Physiol*. 1891;1891:549-552.
31. Shiromoto Y, Kuramochi-Miyagawa S, Daiba A, et al. GPAT2, a mitochondrial outer membrane protein, in piRNA biogenesis in germline stem cells. *RNA*. 2013;19(6):803-810. https://doi.org/10.1261/rna.038521.113
32. Zhang J, Wang Q, Wang M, et al. GASZ and mitofusin-mediated mitochondrial functions are crucial for spermatogenesis. *EMBO Rep*. 2016;17(2):220-234. doi:10.15252/embr.201540846
33. Saxe JP, Chen M, Zhao H, Lin H. Tdrkh is essential for spermatogenesis and participates in primary piRNA biogenesis in the germline. *EMBO J*. 2013;32(13):1869-1885. https://doi.org/10.1038/emboj.2013.121
34. Xiol J, Cora E, Koglgruber R, et al. A role for Fkbp6 and the chaperone machinery in piRNA amplification and transposon silencing. *Mol Cell*. 2012;47(6):970-979. https://doi.org/10.1016/j.molcel.2012.07.019
35. Kuramochi-Miyagawa S, Watanabe T, Gotoh K, et al. DNA methylation of retrotransposon genes is regulated by Piwi family members MILI and MIWI2 in murine fetal testes. *Genes Dev*. 2008;22(7):908-917. https://doi.org/10.1101/gad.1640708
36. Hensen F, Moretton A, van Esveld S, Farge G, Spelbrink JN. The mitochondrial outer-membrane location of the EXD2 exonuclease contradicts its direct role in nuclear DNA repair. *Sci Rep*. 2018;8(1):5368. https://doi.org/10.1038/s41598-018-23690-y
37. Oehl-Jaschkowitz B, Vanakker OM, De Paepe A, et al. Deletions in 14q24.1q24.3 are associated with congenital heart defects, brachydactyly, and mild intellectual disability. *Am J Med Genet A*. 2014;164(3):620-626. https://doi.org/10.1002/ajmg.a.36321

SUPPORTING INFORMATION

Additional supporting information can be found online in the Supporting Information section at the end of this article.

How to cite this article: Olotu O, Dowling M, Homolka D, et al. Intermitochondrial cement (IMC) harbors piRNA biogenesis machinery and exonuclease domain-containing proteins EXD1 and EXD2 in mouse spermatocytes. *Andrology*. 2023;1-14. https://doi.org/10.1111/andr.13361